

# Iterative Source-Channel Decoding With Markov Random Field Source Models

Jörg Kliewer, *Senior Member, IEEE*, Norbert Goertz, *Senior Member, IEEE*, and Alfred Mertins, *Senior Member, IEEE*

**Abstract**—We propose a joint source-channel decoding approach for multidimensional correlated source signals. A Markov random field (MRF) source model is used which exemplarily considers the residual spatial correlations in an image signal after source encoding. Furthermore, the MRF parameters are selected via an analysis based on extrinsic information transfer charts. Due to the link between MRFs and the Gibbs distribution, the resulting soft-input soft-output (SISO) source decoder can be implemented with very low complexity. We prove that the inclusion of a high-rate block code after the quantization stage allows the MRF-based decoder to yield the maximum average extrinsic information. When channel codes are used for additional error protection the MRF-based SISO source decoder can be used as the outer constituent decoder in an iterative source-channel decoding scheme. Considering an example of a simple image transmission system we show that iterative decoding can be successfully employed for recovering the image data, especially when the channel is heavily corrupted.

**Index Terms**—EXIT charts, iterative source-channel decoding, joint source-channel coding, Markov random fields.

## I. INTRODUCTION

**D**UE to Shannon's separation principle, source and channel coding can be carried out independently without any loss in performance when the block length tends to infinity. Since even for finite block lengths, this principle has turned out to be quite reasonable, it is generally applied to the design of many practical communication systems. However, recently joint source-channel coding approaches have become a good alternative especially for the delay- and complexity-constrained transmission of multimedia data content. One subclass of those approaches is given by joint source-channel decoding [1], [2], where residual source redundancy is exploited for additional error protection at the decoder. Some approaches even do not use channel codes at all and design the source encoder such that the residual index-based redundancy in the resulting bit stream alone is sufficient to provide reasonable error protection at

the decoder (e.g., [3]–[5]). These methods have less encoding delay and complexity and, for decreasing signal-to-noise ratios (SNRs) on the communication channel, they exhibit a graceful-degradation behavior and thus often yield similar or better performance for strongly distorted channels than the combination of strong source and channel encoding (e.g., [6]–[8]).

On the other hand, postprocessing error concealment methods have become part of most decoders for noisy environments and channels with erasures [9]–[12]. Techniques applicable to blockwise transmission of single images estimate the content of missing or damaged blocks from adjacent blocks using smoothness constraints or Bayesian approaches [10]–[12]. A special form of Bayesian reconstruction was introduced by Geman and Geman in [13], who applied Markov random field theory and the Markov–Gibbs correspondence for describing the *a priori* information of images in order to obtain maximum *a posteriori* (MAP) image estimates. Their method and many follow-up schemes are suitable for general image restoration applications and not only for error concealment in video or image transmission.

In this paper, we propose a soft-input soft-output (SISO) decoder for noisy images based on Markov random fields (MRFs) that exploits the two-dimensional (2-D) residual spatial redundancy of quantized source images as well as redundancy introduced by channel codes. The benefit of this source decoder is that by applying the Markov–Gibbs correspondence, it can be realized with very low complexity. Furthermore, using MRF models, no source statistics must be transmitted or stored at the decoder except for a few MRF parameters. This is in contrast to a BCJR-style [14] decoding approach, which directly exploits the transition probabilities of the quantized image pixels in the decoder (e.g., as in [4], [5], and [15]–[17]). As an extension of previous work on MRF-based decoding [18]–[20], we demonstrate how the parameters of the underlying MRF can be selected by maximizing the average bitwise mutual information between the original quantized image data and the soft-output data of the source decoder. We show that, in combination with channel codes, the MRF-based SISO decoder can then be used as constituent decoder in an iterative source-channel decoding scheme for robust image transmission. As a further new result, we show that the performance of the MRF-based source decoder in an iterative environment can be improved by applying a high-rate block code after quantization and jointly decoding the block code and the image while using the MRF modeling in the source decoder.

The outline of the paper is as follows. In Section II, the underlying transmission system is described. Section III presents

Manuscript received November 23, 2004; revised October 26, 2005. The associate editor coordinating the review of this manuscript and approving it for publication was Dr. David J. Miller. This work was in part supported by the German Research Foundation (DFG) under grant KL1080/3-1. This paper was presented in part at the ITG Conference on Source and Channel Coding (SCC), Erlangen, Germany, January 2004, and at the IEEE Conference on Acoustics, Speech, and Signal Processing (ICASSP), Montreal, QC, Canada, May 2004.

J. Kliewer is with the Department of Electrical Engineering, University of Notre Dame, Notre Dame, IN 46556 USA (e-mail: jkliewer@nd.edu).

N. Goertz is with the Institute for Digital Communications, Joint Research Institute for Signal & Image Processing, The University of Edinburgh, Edinburgh, EH9 3JL, U.K. (e-mail: norbert.goertz@ed.ac.uk).

A. Mertins is with the Department of Physics, University of Oldenburg, 26111 Oldenburg, Germany (e-mail: alfred.mertins@uni-oldenburg.de).

Digital Object Identifier 10.1109/TSP.2006.879330

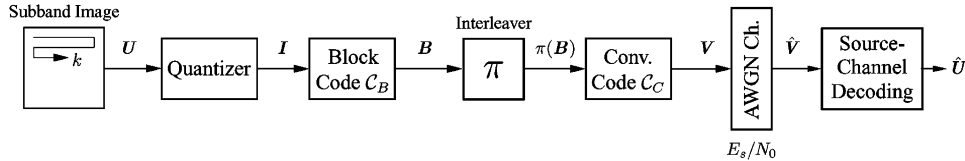


Fig. 1. Model of the transmission system.

a robust MRF-based SISO source-decoding algorithm where an iterative procedure is proposed by using the Markov–Gibbs correspondence. Section IV discusses the resulting iterative source channel decoder when convolutional channel codes are used for additional error protection. In particular, the performance of the MRF-based SISO source decoder is evaluated for different parameter settings via extrinsic information transfer (EXIT) charts [21], [22], which are also employed for assessing the convergence behavior of the iterative decoding scheme. As one of the results of this analysis, we show how the average extrinsic information available at the MRF-based decoder can be increased through the use of slightly redundant alphabets. Section V demonstrates the potential of the proposed MRF approach by presenting some performance results for the transmission of images over noisy channels. Finally, the conclusions are offered in Section VI.

## II. NOTATION AND TRANSMISSION SYSTEM

Random variables (RVs) are denoted with capital letters and their corresponding realizations with lowercase letters. Sequences of random variables and realizations are indicated by boldface italic letters (as “ $\mathbf{U}$ ” or “ $\mathbf{u}$ ”). Furthermore, boldface roman letters denote matrices and vectors. A vector or sequence index is denoted with the index “ $k$ ” and a bit-index with “ $\ell$ .” A lowercase  $p(\cdot)$  denotes a probability density function (pdf), and the uppercase  $P(\cdot)$  a probability mass function.

The block diagram of the overall transmission system is depicted in Fig. 1. The 2-D subband image is scanned in order to obtain the one-dimensional (1-D) subband vector  $\mathbf{U} = [U_1, U_2, \dots, U_Q]$  consisting of  $Q$  source symbols  $U_k$ ,  $k = 1, \dots, Q$ . After subsequent (vector-)quantization, the resulting realizations  $i_k$  of the RVs  $I_k$  are represented with  $M$  bits and thus are elements of the finite alphabet  $\mathcal{I} = \{0, 1, \dots, 2^M - 1\}$ , where a natural mapping is used for the quantizer indexes  $I_k$ . We can generally assume that there are dependencies between the elements of the index vector  $\mathbf{I} = [I_1, I_2, \dots, I_Q]$  due to delay and complexity constraints in the quantization stage. Then, a rate  $R_B = M/N$  systematic binary block encoder  $\mathcal{C}_B^1$  with generator matrix  $\mathbf{G} = [\mathbf{I}_M \ \mathbf{F}]$  is applied to each source index  $I_k$ . Herein,  $\mathbf{I}_M$  denotes the  $M \times M$  identity matrix, and  $\mathbf{F} \in \{0, 1\}^{M \times (N-M)}$  generates the parity bit vector  $\mathbf{p}_k = \mathbf{i}_k^T \mathbf{F} = [p_{k,1}, p_{k,2}, \dots, p_{k,(N-M)}]^T$ , where  $\mathbf{i}_k$  describes the realization  $i_k \in \mathcal{I}$  as an  $M$ -bit binary vector. This leads to the  $N$ -bit codewords  $[\mathbf{i}_k \ \mathbf{p}_k]$  which, for convenience, may also be written in index notation as  $b_k = [i_k \ p_k]$ , where  $p_k$  is the  $(N - M)$ -bit index corresponding to the vector  $\mathbf{p}_k$ . The realizations  $b_k$  are elements of the set of all  $2^M$  number of possible codewords  $\mathcal{B}$ , and the corresponding processes are

denoted by  $B_k = [I_k \ P_k]$ . The concatenation of the indexes  $B_k$  for all  $k$  leads to the index sequence  $\mathbf{B}$ , which is bit-interleaved prior to convolutional channel encoding using the systematic encoder  $\mathcal{C}_C$  with rate  $R_C$ .

The reason for introducing the code  $\mathcal{C}_B$  in Fig. 1 is that after additional (high-rate) block encoding, the minimum distance for the resulting codewords  $b_k$  is increased. This can be exploited in an iterative source-channel decoder setup if MRF source model and block code are jointly SISO decoded in an outer joint source-channel decoder, as we will show in Section IV. Note that if the codes  $\mathcal{C}_B$  and  $\mathcal{C}_C$  were interpreted as a serially concatenated code in Fig. 1, iterations would need to be performed between the iterative decoder for the concatenation of  $\mathcal{C}_B$  and  $\mathcal{C}_C$  and the source decoder. However, such a setup reduces the performance of the overall decoder since the serial concatenation represents a very strong component code, and, in contrast, the source decoder (without considering  $\mathcal{C}_B$ ) suffers from a poor minimum distance of one between the source indexes  $i_k$ .

After applying  $\mathcal{C}_C$ , we obtain the code bit sequence  $\mathbf{V} = [V_1, V_2, \dots, V_{Q_v}]$  with  $Q_v = Q \cdot M / (R_C \cdot R_B)$  and  $V_\ell$ ,  $\ell = 1, 2, \dots, Q_v$ , denoting the RV for a single bit. This bit sequence is then transmitted over a binary phase-shift keying (BPSK) modulated additive white Gaussian noise (AWGN) channel. The conditional pdf for the received soft bit  $\hat{V}_\ell$  with  $\hat{v}_\ell \in \mathbb{R}$  at the channel output given the transmitted bit  $v_\ell$  can be written as

$$p(\hat{v}_\ell | v_\ell) = \frac{1}{\sqrt{2\pi\sigma_e^2}} e^{-\frac{1}{2\sigma_e^2}(\hat{v}_\ell - v_\ell)^2}, \quad v_\ell = 1 - 2v_\ell, \quad \hat{v}_\ell \in \mathbb{R} \quad (1)$$

with  $\sigma_e^2 = (N_0/2E_s)$  denoting the channel noise variance.  $E_s$  is the energy used to transmit each bit, and  $N_0$  corresponds to the one-sided power spectral density of the noise. Using conditional log-likelihood ratios (L-values), we may express (1) also as

$$L(\hat{v}_\ell | v_\ell) = \ln \left( \frac{p(\hat{v}_\ell | v_\ell = 0)}{p(\hat{v}_\ell | v_\ell = 1)} \right) = 4 \frac{E_s}{N_0} \hat{v}_\ell = L_c \hat{v}_\ell \quad (2)$$

with the constant  $L_c = 4(E_s/N_0)$ . The source-channel decoding step in Fig. 1 then provides an estimate  $\hat{\mathbf{U}}$  of the input vector  $\mathbf{U}$ .

## III. MRF-BASED SISO SOURCE DECODING

In this section, the implicit residual redundancy after source encoding and the explicit redundancy from the block code  $\mathcal{C}_B$  in Fig. 1 are jointly exploited for error protection in the source decoder. Thus, the encoder  $\mathcal{C}_C$  shown in the transmission system in Fig. 1 is assumed not to be present, and we therefore have  $\mathbf{V} = \mathbf{B}$ . Of course, the encoder  $\mathcal{C}_C$  is used later on in the iterative decoder described in Section IV.

<sup>1</sup>Note that a nonsystematic encoder may be used here as well.

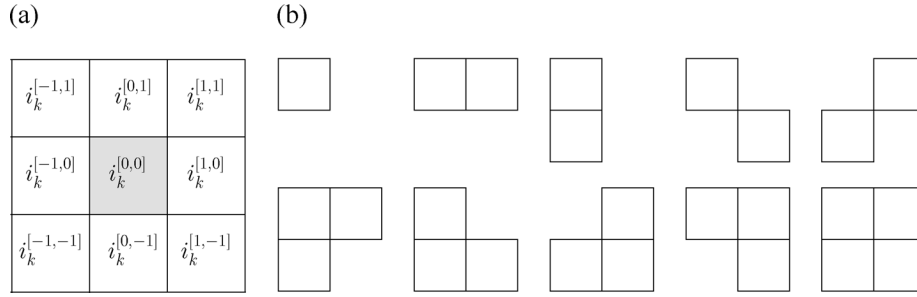


Fig. 2. (a) Eight-pixel neighborhood system; (b) all ten corresponding cliques where  $i_k^{[0,0]}$  can be in any of the boxes.

The SIS0 source decoder derived in the following is based on a MRF source model which generates *a posteriori* probabilities (APPs) for the source hypotheses  $I_k = i_k$ . To this end, let us consider the eight nearest neighbors for a given subband source index  $i_k$  within a quantized subband image prior to transmission. Such a neighborhood system is displayed in Fig. 2(a), where all neighboring source indexes are referenced relatively to the index  $i_k^{[0,0]}$  under consideration. For the sake of brevity, the quantity  $i_k^{[0,0]}$  will also simply be written as  $i_k$  in the following. Furthermore, we denote the set of all source indexes belonging to the neighborhood of  $i_k$  as  $\mathcal{N}_{i_k} = \{i_k^{[q,j]} : q, j = -1, 0, 1 \setminus q = j = 0\}$ . Since, in principle, all indexes in the neighborhood system of Fig. 2(a) show spatial dependencies due to imperfect source encoding the index probabilities  $P(i_k)$ ,  $i_k \in \mathcal{I}$  may be modeled via a MRF using the well-known Markov–Gibbs correspondence [13]. Using this relationship, the probability for an element  $i_k$  of the MRF given all other source indexes in a local neighborhood  $\mathcal{N}_{i_k}$  can then be stated as [13]

$$P(i_k | \mathcal{N}_{i_k}) = \frac{1}{Z} e^{-\frac{1}{T} U(i_k, \mathcal{N}_{i_k})} \quad (3)$$

where the function  $U(i_k, \mathcal{N}_{i_k})$  is called the energy function, the quantity  $T$  is called the temperature, and  $Z$  denotes a normalization constant. We can decompose  $U(i_k, \mathcal{N}_{i_k})$  into a sum over so-called potential functions  $V_C(i_k, \mathcal{N}_{i_k})$  according to

$$U(i_k, \mathcal{N}_{i_k}) = \sum_C V_C(i_k, \mathcal{N}_{i_k}). \quad (4)$$

The potential functions are defined for given cliques  $C$ , and the summation in (4) is carried out over all possible cliques in the local neighborhood  $\mathcal{N}_{i_k}$  or over a subset of all possible cliques. Within a clique, every site must be in the neighborhood of all other sites, or it is a singleton with just one site. For the eight-pixel neighborhood system in Fig. 2(a), all associated cliques are shown in Fig. 2(b). The first type of clique just consists of single source indexes, the second type of cliques describes the index  $i_k$  and its horizontal neighbors, the third type addresses all vertical neighbors of  $i_k$ , and so on.

In the image restoration literature, it is common to restrict the potential functions to certain types and to choose only a subset of all possible cliques in order to model images (e.g., [13] and [23]). Although such restricted models do not allow for an exact representation of all MRFs via the selected Gibbs distribution, they still yield very good, yet simple models of natural images.

In the following, the generalized Gaussian image model introduced by Bouman and Sauer in [23] is used. This model choice is supported by the fact that the wavelet coefficients of natural images (except for the lowpass subband) have been found to follow a generalized Gaussian distribution [24]. Experimental results [18], [23] indicate that the model yields better performance in Bayesian image restoration and soft-bit-based image reconstruction of natural images than other known models. With this model choice, the potential functions used for two-element cliques are given by the absolute value of the difference of two symbols  $i_k$  and  $i_k^{[q,j]}$ , raised to the power  $\delta$ , where  $\delta$  is a free parameter

$$V_C(i_k, i_k^{[q,j]}) = |i_k - i_k^{[q,j]}|^\delta, \quad [q,j] \neq [0,0]. \quad (5)$$

For  $\delta = 2$ , the model is Gaussian, and for  $\delta = 1$ , it is Laplacian. When using the generalized Gaussian model during MRF-based image restoration, the smaller the value of  $\delta$ , the better the preservation of sharp edges will be [23]. On the other hand, reducing  $\delta$  comes at the cost of less noise reduction in smooth image areas, so that a compromise between edge preservation and noise reduction capability must be found. A value of  $\delta$  around one (or slightly smaller) often yields a good match for natural images. In [18], the value of  $\delta = 0.7$  was experimentally found to be a good choice for soft-bit-based image restoration.

In the present paper, we carry out the parameter selection based on an EXIT-chart analysis, where the details will be discussed in Section IV-C. In this context, we also investigate the inclusion of three-element cliques using the potential function

$$V_C(i_k, i_k^{[q_1, j_1]}, i_k^{[q_2, j_2]}) = |2i_k - i_k^{[q_1, j_1]} - i_k^{[q_2, j_2]}|^\delta, \quad [q_1, j_1], [q_2, j_2] \neq [0,0], \quad [q_1, j_1] \neq [q_2, j_2] \quad (6)$$

which can be seen as an extension of (5). Furthermore, single-element cliques are not used in this paper.

In order to apply the MRF model to the source decoder, we consider the neighborhood  $\mathcal{N}_{i_k}^{\tilde{z}} = \{i_k^{[q,j]} : q, j = -1, 0, 1 \setminus q = j = 0\}$  where  $i_k^{[q,j]} \in \mathcal{I}$  denotes an *already decoded* estimate of  $i_k^{[q,j]}$ , for example from a previous maximum-likelihood (ML) decoding of the received soft-bits at the channel output. The APPs for the index realization  $i_k$  based on the local neighborhood at the decoder can then be written as  $P(i_k | \hat{\mathbf{b}}_k, \mathcal{N}_{i_k}^{\tilde{z}})$ , where the soft-bit sequence realization  $\hat{\mathbf{b}}_k = [\hat{b}_{k,1}, \hat{b}_{k,2}, \dots, \hat{b}_{k,N}]$  consists of the individual soft-bits  $\hat{b}_{k,\ell} \in \mathbb{R}$  received at the output

of the AWGN channel. By applying Bayes' theorem, and by additionally considering the memoryless property of the channel and the systematic property of  $\mathcal{C}_B$ , we obtain

$$\begin{aligned} P\left(i_k|\hat{\mathbf{b}}_k, \mathcal{N}_{i_k}^{\tilde{z}}\right) &= c_k \cdot p\left(\hat{\mathbf{b}}_k|b_k(i_k)\right) P\left(i_k|\mathcal{N}_{i_k}^{\tilde{z}}\right) \\ &= c_k \cdot p(\hat{\mathbf{i}}_k|i_k)p(\hat{\mathbf{p}}_k|p_k)P\left(i_k|\mathcal{N}_{i_k}^{\tilde{z}}\right) \end{aligned} \quad (7)$$

with the normalization constant

$$c_k = \frac{1}{p(\hat{\mathbf{b}}_k)}, \quad p(\hat{\mathbf{b}}_k) = \sum_{i_k=0}^{2^M-1} p\left(\hat{\mathbf{b}}_k|b_k(i_k)\right) P\left(i_k|\mathcal{N}_{i_k}^{\tilde{z}}\right) \quad (8)$$

and  $p_k \in \{0, 1, \dots, 2^{N-M} - 1\}$ . The quantities  $\hat{\mathbf{i}}_k$  and  $\hat{\mathbf{p}}_k$ , with  $\hat{\mathbf{b}}_k = [\hat{\mathbf{i}}_k, \hat{\mathbf{p}}_k]$ , are soft-bit sequences received at the channel output that correspond to the transmitted sequences of index and parity bits, respectively. For brevity of notation and for use in (5), we employ the equivalent index notations  $i_k$  and  $p_k$  for the hypotheses of both the transmitted index and parity bits. Note that  $p_k$  deterministically depends on the index  $i_k$  due to the channel code  $\mathcal{C}_B$ . In (7), the pdf's  $p(\hat{\mathbf{i}}_k|i_k)$  and  $p(\hat{\mathbf{p}}_k|p_k)$  represent the soft information at the output of the AWGN channel according to

$$\begin{aligned} p(\hat{\mathbf{i}}_k|i_k) &= \prod_{\ell=1}^M p(\hat{i}_{k,\ell}|i_{k,\ell}) \quad \text{and} \\ p(\hat{\mathbf{p}}_k|p_k) &= \prod_{\ell=1}^{N-M} p(\hat{p}_{k,\ell}|p_{k,\ell}). \end{aligned} \quad (9)$$

The conditional pdf  $p(\hat{i}_{k,\ell}|i_{k,\ell})$  for the  $\ell$ th bit  $i_{k,\ell}$  of the index  $i_k$  is given in (1) when  $v_\ell$  is replaced with  $i_{k,\ell}$ , where the same holds for the  $\ell$ th parity bit  $p_{k,\ell}$ . The term  $P(i_k|\mathcal{N}_{i_k}^{\tilde{z}})$  in (7) corresponds to the conditional probability from (3) where the original source indexes  $i_k^{[q,j]}$  for the neighborhood are replaced by the estimates  $\tilde{i}_k^{[q,j]}$ .

Like in classical Bayesian MRF-based image restoration [13], we use an iterative decoding approach where (7) is applied multiple times until convergence is achieved. In each iteration, the sites within a subband are visited sequentially, following the scanning path in Fig. 1, and updates are applied immediately. The procedure is as follows.

- 1) Obtain initial estimates  $\tilde{i}_k^{(0)}$  for the received 1-D scanned subband image indexes by performing an ML decoding from the received soft-bit sequence  $\hat{\mathbf{b}}_k$  at the channel output. Set  $r \leftarrow 0$ .
- 2) Apply (7) with (3), (4), and (5) in order to determine the APPs  $P(i_k|\hat{\mathbf{b}}_k, \mathcal{N}_{i_k}^{\tilde{z}(r)})$ .
- 3) Obtain a new estimate  $\tilde{i}_k^{(r+1)}$  via a MAP estimation according to

$$\tilde{i}_k^{(r+1)} = \arg \max_{i_k} P\left(i_k|\hat{\mathbf{b}}_k, \mathcal{N}_{i_k}^{\tilde{z}(r)}\right).$$

- 4) Set  $r \leftarrow r + 1$  and go to Step 2) unless the difference between estimates  $\tilde{i}_k^{(r)}$  and  $\tilde{i}_k^{(r+1)}$  lies below a certain threshold or a maximum number of iterations is exceeded.

The overall number of MRF decoder iterations will be denoted as  $N_{i,\text{MRF}}$ , where a single decoder pass corresponds to  $N_{i,\text{MRF}} = 0$ .

In our experiments, we always have observed that the above algorithm converges to a fix point, however, convergence to a global optimum cannot be guaranteed.

The resulting APPs  $P(i_k|\hat{\mathbf{b}}_k, \mathcal{N}_{i_k}^{\tilde{z}(N_{i,\text{MRF}})})$  at the output of the last iteration may be interpreted as APPs  $P(i_k|\hat{\mathbf{b}}_k, \mathcal{N}_{i_k}^{\tilde{z}})$  depending on all received soft-bit vectors  $\tilde{\mathbf{i}}_k^{[q,j]}$  in the local neighborhood of  $\hat{\mathbf{i}}_k$ . The reconstructed source values  $\hat{u}_k$  are then estimated via a mean-squares (MS) estimation such that

$$\hat{u}_k = \arg \min_{\hat{u}_k} E \left\{ d(U_k, \hat{u}_k) | \hat{\mathbf{b}}_k, \mathcal{N}_{i_k}^{\tilde{z}} \right\} \quad (10)$$

where for the distortion measure  $d(\cdot, \cdot)$ , the squared Euclidean distance is used. For this distance, the value  $\hat{u}_k$  maximizing the reconstruction SNR is given by the conditional expectation of the RV  $U_k$  as

$$\hat{u}_k = \sum_{i=0}^{2^M-1} u_q(i) \cdot P\left(i|\hat{\mathbf{b}}_k, \mathcal{N}_{i_k}^{\tilde{z}}\right) \quad (11)$$

which uses the APPs computed by the source decoder. Herein,  $u_q(i)$  denotes the quantizer reconstruction levels corresponding to the source hypotheses  $I_k = i$ .

The proposed MRF source decoder with APPs calculated in the logarithmic domain has a complexity of approximately

$$2^M (3N + N_C (c_\delta + N_E^2 + N_E - 5) (N_{i,\text{MRF}} + 1)) = O(2^M) \quad (12)$$

arithmetic operations<sup>2</sup> per source index, where  $N_C$  denotes the number of cliques,  $N_E$  the maximum number of considered elements in a single clique,<sup>3</sup> and  $c_\delta$  a fixed number of operations for computing the raise to the power of  $\delta$ . Note that from the total number of arithmetic operations in (12), roughly a number of  $2^{M+1}(N - M)$  operations is due to the decoding of the block code  $\mathcal{C}_B$ . In contrast, the SISO source decoding approach from [25], where horizontal and vertical correlations in the subband image are considered as separate Markov sources, has a significantly higher complexity of approximately  $4 \cdot 2^{2M}(2M + 1) = O(2^{2M})$  operations per source index. A similar approach has been stated in [16], where the computed APPs depend on all horizontal and vertical neighbors, and not only on the nearest ones, of the actual index under consideration. In addition, in the latter approach, in contrast to the proposed MRF-based source decoder, transition probabilities for the source hypotheses must be trained and stored in the decoder, which leads to an additional demand of resources. As an example, for a typical setting using the parameters  $M = 5$  bits,  $N = 6$  bits,  $N_E = 2$  elements per clique,  $N_C = 8$  cliques,  $N_{i,\text{MRF}} = 1$  iteration, and  $c_\delta = 10$  operations, the MRF source decoder can be realized in approximately 6200 operations per source index according to (12),

<sup>2</sup>These could be either additions or multiplications.

<sup>3</sup>All potential functions with a smaller amount of elements except singletons are considered in the evaluation of (4) as well.

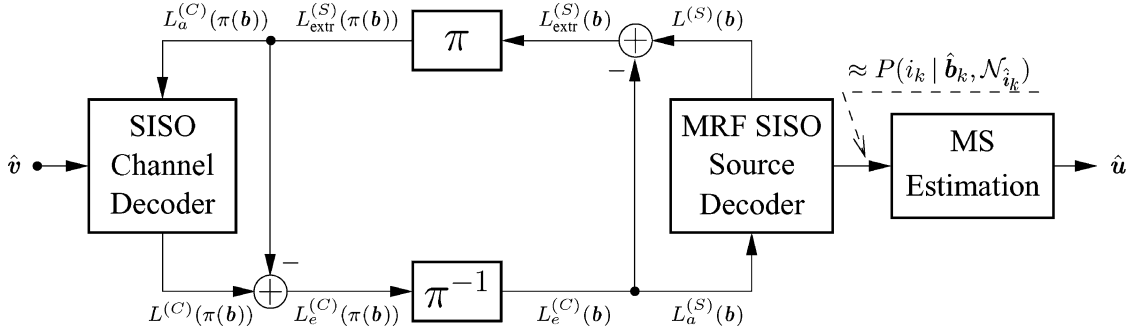


Fig. 3. Structure of the iterative source-channel decoder.

whereas the method from [25] requires over 65 000 operations per source index.

The selection of the MRF parameters is carried out via EXIT characteristics and will be discussed in the following section.

#### IV. ITERATIVE SOURCE-CHANNEL DECODING

##### A. Decoder Structure

An error protection carried out by using only the residual spatial source redundancy and a high-rate block code may not be enough in many transmission situations. Therefore, we assume that the output of the source encoder is protected by a systematic convolutional code  $\mathcal{C}_C$ , as it is depicted in Fig. 1. Note that this scheme is highly similar to a serially concatenated channel code. Therefore, we can apply an iterative decoding scheme [17], [26], where the outer constituent channel decoder is replaced by the MRF-based source decoder presented in Section III.

The structure of the resulting decoder is depicted in Fig. 3. At the beginning of the first iteration, the SISO channel decoder issues APPs  $P(b'_{k,\ell}|\hat{\mathbf{v}})$  for the source-encoded bits  $b'_{k,\ell}$  taken from a realization  $\pi(\mathbf{b})$  of the bit-interleaved sequence  $\pi(\mathbf{B})$ . These APPs are used to calculate the corresponding conditional L-values  $L^{(C)}(b'_{k,\ell}) := \ln(P(b'_{k,\ell} = 0|\hat{\mathbf{v}})/P(b'_{k,\ell} = 1|\hat{\mathbf{v}}))$ . It is shown in [27] that the L-values can be written as  $L^{(C)}(b'_{k,\ell}) = L_c \hat{b}'_{k,\ell} + L_a^{(C)}(b'_{k,\ell}) + L_{\text{extr}}^{(C)}(b'_{k,\ell})$  for  $\ell = 1, 2, \dots, N$ ,  $k = 1, 2, \dots, Q$ . The term  $L_c \hat{b}'_{k,\ell}$  is defined analog to (2) for the interleaved source codebits  $b'_{k,\ell}$  at the source decoder output. The quantity  $L_a^{(C)}(b'_{k,\ell})$  denotes the *a priori* information for the bit  $b'_{k,\ell}$ , and  $L_{\text{extr}}^{(C)}(b'_{k,\ell})$  refers to the extrinsic information. After subtraction of the *a priori* term and after deinterleaving, we obtain the L-values  $L_e^{(C)}(b_{k,\ell}) = L_c \hat{b}_{k,\ell} + L_{\text{extr}}^{(C)}(b_{k,\ell})$ , which are used as *a priori* information  $L_a^{(S)}(b_{k,\ell})$  for the SISO source decoder. In the following, we assume that all bits  $b_{k,\ell}$  are mutually independent. Then, the corresponding index-based probabilities for the *a priori* L-values  $L_a^{(S)}(b_{k,\ell})$  can be obtained by bitwise multiplication of the probabilities for the bits  $b_{k,\ell}$ . By inserting this *a priori* knowledge into (7), we obtain the following APPs, which are now also conditioned on the sequence  $\hat{\mathbf{v}}$ , as

$$P(i_k|\hat{\mathbf{b}}_k, \mathcal{N}_{i_k}^z, \hat{\mathbf{v}}) = \bar{c}_k \cdot P(i_k|\mathcal{N}_{i_k}^z) \cdot \prod_{\ell=1}^N p(\hat{b}_{k,\ell}|b_{k,\ell} = \mathbf{i}_k^T \mathbf{g}_\ell) P_{\text{extr}}^{(C)}(b_{k,\ell} = \mathbf{i}_k^T \mathbf{g}_\ell|\hat{\mathbf{v}}). \quad (13)$$

Herein,  $\bar{c}_k$  is a normalization constant (as in (8)) and  $\mathbf{g}_\ell$  is the  $\ell$ th column vector of the generator matrix  $\mathbf{G}$ .

The initial estimates  $\hat{i}_k^{(0)}$  for the iterative MRF-based source decoding procedure described in Section III can be derived from the deinterleaved L-values  $L^{(C)}(b_{k,\ell})$  by first converting these L-values into APPs for the bits  $b_{k,\ell}$ . Then, by multiplying these probabilities for all  $\ell$ , we obtain index-based APPs  $P(i_k|\hat{\mathbf{v}})$  from which  $\hat{i}_k^{(0)}$  can be computed via an MS estimation according to (11). Requantizing  $\hat{i}_k^{(0)}$  with  $M$  bits yields the index  $\hat{i}_k^{(0)}$ .

After the iterations within the MRF-based source decoder have been performed, the output of the SISO source decoder corresponds to index-based APPs  $P(i_k|\hat{\mathbf{b}}_k, \mathcal{N}_{i_k}^z, \hat{\mathbf{v}})$ , where the related bit-based L-values can be derived for  $\ell = 1, 2, \dots, N$  as

$$L^{(S)}(b_{k,\ell}) = \ln \left( \frac{\sum_{\forall i_k \in \mathcal{I}: \mathbf{i}_k^T \mathbf{g}_\ell = 0} P(i_k|\hat{\mathbf{b}}_k, \mathcal{N}_{i_k}^z, \hat{\mathbf{v}})}{\sum_{\forall i_k \in \mathcal{I}: \mathbf{i}_k^T \mathbf{g}_\ell = 1} P(i_k|\hat{\mathbf{b}}_k, \mathcal{N}_{i_k}^z, \hat{\mathbf{v}})} \right). \quad (14)$$

By subtracting the source *a priori* information  $L_a^{(S)}(b_{k,\ell})$  from  $L^{(S)}(b_{k,\ell})$  in (14), we finally obtain the extrinsic information  $L_{\text{extr}}^{(S)}(b_{k,\ell})$ , which is used as *a priori* information for subsequent channel decoding. As in all iterative decoding schemes, the constituent decoders (SISO source decoder and SISO channel decoder in our case) are alternately run several times, until convergence or nonconvergence is detected by a suitable stopping criterion (see, e.g., [27]). We here employ a very simple criterion: decoding is stopped if the average extrinsic information at each constituent decoder, which will be defined in (15) and (16) in the next subsection, is not increasing anymore between subsequent iterations or if a given maximum number of iterations is reached. Note that in our setup, we have two types of iterations: the turbo-like decoding iterations and the iterations within the MRF-based source decoder.

##### B. EXIT Characteristics

In order to analyze the iterative decoding process and also to determine the appropriate parameters for the MRF-based source decoder, an EXIT chart analysis [21], [22] is applied to the above iterative decoder. EXIT charts visualize the input/output characteristics of the constituent SISO decoders in terms of an average mutual information transfer between the bits  $b_{k,\ell}$  of the transmitted index sequence  $\mathbf{b}$  and the *a priori* information

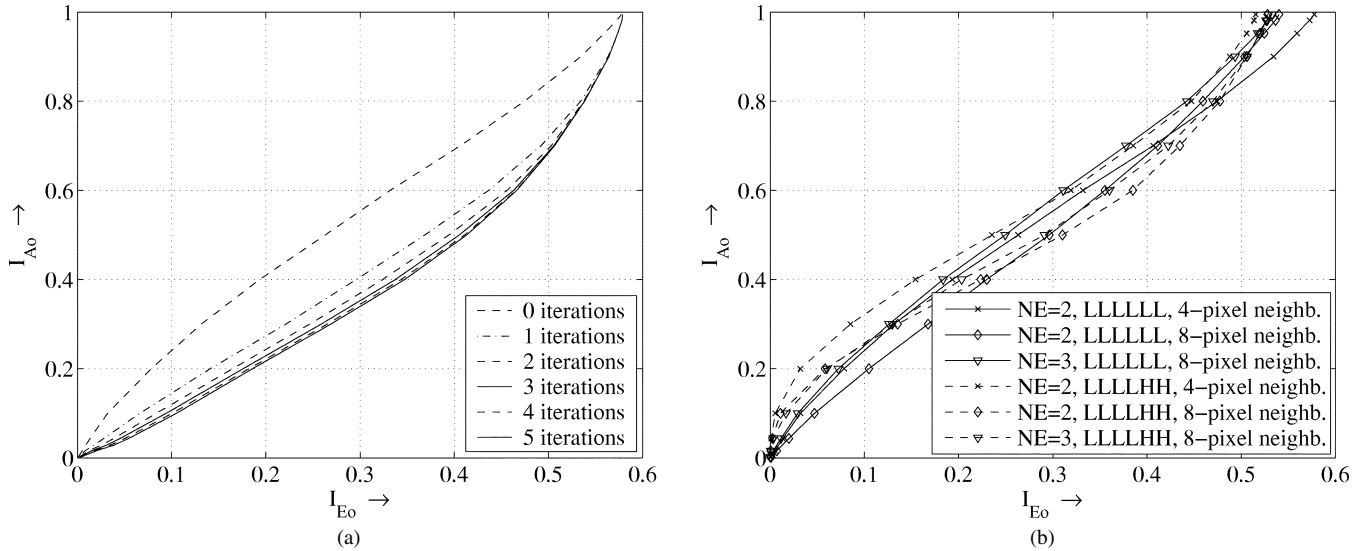


Fig. 4. Transfer functions  $T_o$  for the MRF-based source decoder (“Goldhill” test image,  $M = 6$  bits): (a) dependency of the number of iterations  $N_{i,MRF}$  in the source decoder ( $T = 1$ ,  $\delta = 0.5$ , LLLLLL subband,  $N_E = 2$  with four-pixel neighborhood (horiz./vert.)); (b) dependency on the size of the neighborhood region for  $N_{i,MRF} = 0$  (LLLLLL subband:  $T = 1$ ,  $\delta = 0.5$  for  $N_E = 2$ ;  $T = 1.5$ ,  $\delta = 0.2$  for  $N_E = 3$ . LLLLHH subband:  $T = 3$ ,  $\delta = 0.5$  for  $N_E = 2$ ;  $T = 1$ ,  $\delta = 0.1$  for  $N_E = 3$ ).

$L_a(b_{k,\ell})$ , and between  $b_{k,\ell}$  and  $L_{e/extr}(b_{k,\ell})$  at the output, respectively. Denoting the mutual information between two RVs  $X$  and  $Y$  as  $I(X; Y)$ , we define [21], [22], [28]

$$I_{A_i} := \frac{1}{QN} \sum_{k=1}^Q \sum_{\ell=1}^N I(B'_{k,\ell}; L_a^{(C)}(B'_{k,\ell})) \quad (15)$$

$$I_{E_i} := \frac{1}{QN} \sum_{k=1}^Q \sum_{\ell=1}^N I(B'_{k,\ell}; L_e^{(C)}(B'_{k,\ell}))$$

$$I_{A_o} := \frac{1}{QN} \sum_{k=1}^Q \sum_{\ell=1}^N I(B_{k,\ell}; L_a^{(S)}(B_{k,\ell})) \quad (16)$$

$$I_{E_o} := \frac{1}{QN} \sum_{k=1}^Q \sum_{\ell=1}^N I(B_{k,\ell}; L_{extr}^{(S)}(B_{k,\ell})).$$

Herein, the quantities  $I_{A_i}$  and  $I_{A_o}$  denote the average *a priori* information available at the inner decoder (subscript  $i$ ) and outer decoder (subscript  $o$ ), respectively. Likewise,  $I_{E_i}$  and  $I_{E_o}$  represent the average extrinsic information at the outputs of both decoders.<sup>4</sup> These quantities are defined as bitwise mutual information averaged over a block of  $Q \cdot N$  bits for the inner decoder associated with the code  $\mathcal{C}_C$  and  $N$  bits for the source code, respectively. However, since the source statistic obtained by the Gibbs distribution is nonstationary, the bitwise mutual information in (16) must be averaged over the whole sequence as well. The transfer characteristics of the constituent decoders are now given as

$$I_{E_i} = T_i(I_{A_i}, E_s/N_0) \quad \text{and} \quad I_{E_o} = T_o(I_{A_o}). \quad (17)$$

Note that the transfer characteristic  $T_i$  of the inner decoder is parameterized with the channel parameter  $E_s/N_0$  since *a priori*

<sup>4</sup>Note that  $I_{E_i}$  contains information from both extrinsic L-values and channel observations. However, in accordance with the literature and for the sake of simplicity,  $I_{E_i}$  will be simply denoted as average extrinsic information.

information and channel observation  $\hat{V}$  are employed in the decoding process. For the outer constituent decoder, the *a priori* information represents the only soft-input such that the transfer characteristic  $T_o$  here only depends on  $I_{A_o}$ . Since the *a priori* L-values  $L_a^{(S/C)}(\cdot)$  are assumed to be Gaussian-distributed and uncorrelated [21], [22], we can obtain the functions  $T_i$  and  $T_o$  by applying a Gaussian-distributed random sequence with variance  $\sigma_A^2$  and average mutual information  $I_A$  as *a priori* information to both constituent SISO decoders. The average extrinsic information  $I_E$  is then measured between the extrinsic L-values  $L_{extr}^{(S)}(\cdot)$  or  $L_e^{(C)}(\cdot)$  and  $B_{k,\ell}$  or  $B'_{k,\ell}$  at the output of the constituent decoder. In order to obtain the EXIT chart, both functions  $T_i$  and  $T_o$  can be plotted into one single diagram, where for  $T_o$  the axes are swapped.

### C. EXIT Properties for the MRF-Based Source Decoder

In order to assess the EXIT performance of the MRF-based source decoder, examples for the transfer function  $T_o$  are given for different parameter settings, where all following setups use an  $M = 6$  bits uniform quantization and no extra block code (i.e.,  $\mathbf{G} = \mathbf{I}_M$ ). We assume a three-level wavelet decomposition and exemplarily only consider the four subbands in the lowest decomposition level, which are obtained after both a horizontal and vertical lowpass filtering in the two uppermost levels. These subbands will be denoted with the abbreviations LLLLLL, LL-LLHL, LLLLLH, and LLLLHH, where each letter denotes either a vertical or horizontal lowpass (L) or highpass filtering (H) per decomposition level. Furthermore, both the potential functions in (5) for  $N_E = 2$  and in (6) for  $N_E = 3$  are considered. For the computation of the transfer characteristics, we assume in this work that  $H(B_{k,\ell}) \approx 1$  bit holds. This assumption is fairly well satisfied for the subband indexes of natural source images due to the used natural mapping and an observed symmetric index distribution [24].

Fig. 4(a) depicts the resulting transfer functions for different numbers of iterations  $N_{i,MRF}$  in the MRF *source* decoder for

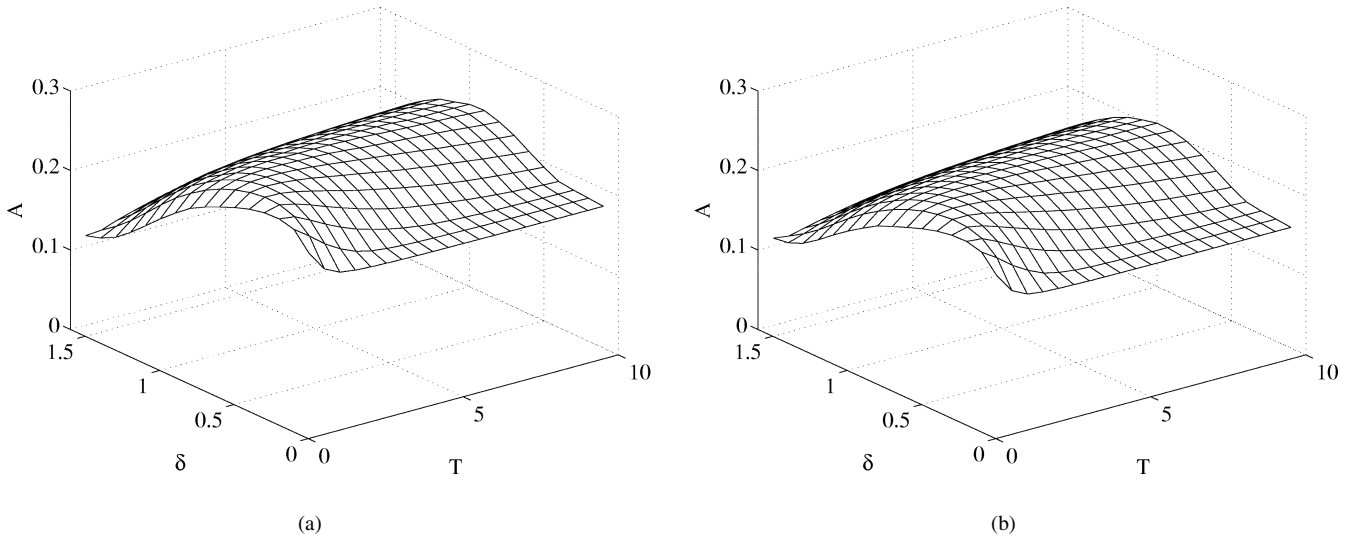


Fig. 5. Area under the EXIT function  $I_{E_o} = T_o(I_{A_o})$  for the MRF-based source decoder (LLLLLL subband quantized with  $M = 6$  bits,  $N_E = 2$ ,  $N_{i,\text{MRF}} = 0$ , three-level wavelet filter bank, 4-pixel neighborhood) (a) “Goldhill” test image, (b) “Barbara” test image.

the LLLLLL subband of the “Goldhill” test image,  $\delta = 0.5$ , and  $T = 1$ , where  $I_{E_o}$  is plotted versus  $I_{A_o}$ . The axes for  $T_o$  are swapped in order to facilitate an incorporation of the inner code characteristic into the diagram. We can observe that the extrinsic information at the decoder output increases for each additional iteration, however, a saturation occurs for more than three iterations. For different subbands, parameter settings, and source images our experiments show a similar behavior, where the strongest increase in extrinsic information is generally observed in the first and second iterations.

Fig. 4(b) shows the dependency on different neighborhood regions for the quantized “Goldhill” lowpass subband of a three-level wavelet filter bank. It can be seen that for the LLLLLL subband a four-pixel neighborhood with two-element cliques, where just the horizontal and vertical neighbors in Fig. 2 are used, leads to the largest average extrinsic information for the point where  $I_{A_o} = 1$  bit (i.e., perfect *a priori* knowledge). However, for  $I_{A_o} < 0.75$  bits the extrinsic information is larger when using the full eight-pixel neighborhood of Fig. 2 with all two-element cliques. Furthermore, as experiments have shown, for images containing more diagonal structures than the “Goldhill” image, the use of diagonal two-element cliques can be beneficial for all values of  $I_{A_o}$ . For the LLLLHH subband of the “Goldhill” image and, as experiments have shown, also for the LLLLHL and LLLLLH subbands an eight-pixel neighborhood and two-element cliques seem to be preferable in terms of the EXIT behavior. In addition, it turns out that due to the different lowpass filtering directions, horizontal dependencies in the LLLLHL subband and vertical dependencies in the LLLLLH subband are stronger than the remaining ones such that a certain weighting between the potential functions for different directions could be introduced. For simplicity, this approach was not considered in the paper.

In order to find the most suitable parameters  $T$  and  $\delta$ , in the following, we consider the area  $A$  under the transfer characteristic  $T_o$  with  $A = \int_0^1 T_o(\xi) d\xi$ . It has been shown in [28] that for a binary erasure channel and a SISO APP decoder, this

area depends on the amount of inserted redundancy described by the code rate  $R$  according to  $A = 1 - R$  for  $H(B_{k,\ell}) = 1$  bit. For AWGN channels, experiments have shown that the approximation  $A \approx 1 - R$  seems to hold [29], even when residual index-based source redundancy is included in the computation of the code rate [30]. Then, for the source encoder, we have  $R = R_B R_S$ . The rate  $R_B$  considers the explicit redundancy due to the code  $\mathcal{C}_B$ , and the source code rate  $R_S = H(\mathbf{I})/M \in [0, 1]$  states the error correction capability of the implicit residual source redundancy, with  $H(\mathbf{I})$  denoting the entropy rate of the sequence  $\mathbf{I}$ . If we now assume that these two redundancy contributions are jointly inserted by a hypothetical channel encoder with block length  $N'$  and code rate  $R$ , the average word error probability  $P_w$  can be upper bounded as  $P_w \leq e^{-N' E_r(R)}$  [31].  $E_r(R)$  represents the random coding or error exponent [31], which is monotonically decreasing for increasing  $R \in [0, C]$ , where  $C$  is the capacity of the channel. If furthermore  $D_Q$  denotes the distortion at the decoder output due to an  $M$ -bit quantization of the image subband data and  $D_{\max}$  the maximal distortion contribution due to flipping one or more bits in the length- $N'$  binary vector  $\mathbf{b}_k$ , an upper bound for the overall output distortion  $D_o$  can be given as

$$D_o \leq D_Q + D_{\max} e^{-N' E_r(R)}. \quad (18)$$

Thus, the maximization of the area  $A$  by properly choosing the MRF parameters is directly associated with a larger lower bound for the reconstruction SNR. This is due to the fact that a larger amount of residual source redundancy can be exploited for error protection.

Fig. 5 shows the area  $A$  versus both parameters  $T$  and  $\delta$ , where Fig. 5(a) displays the results for the quantized LLLLLL subband of the “Goldhill” test image and Fig. 5(b) for the quantized LLLLLL subband of the “Barbara” test image, respectively. It can be observed that a large  $A$  can be obtained for a large range of possible  $(T, \delta)$  pairs, where the individual parameter ranges are quite similar for both images. Table I shows for

TABLE I  
MRF PARAMETERS  $T$  AND  $\delta$  CORRESPONDING TO THE MAXIMAL AREA  $A$  FOR DIFFERENT QUANTIZED SUBBANDS AND TEST IMAGES ( $M = 6$  bits,  $N_{i,\text{MRF}} = 0$ , THREE-LEVEL WAVELET FILTER BANK)

Band	$N_E$	neighborh.	"Goldhill"			"Barbara"			"Lena"		
			$T$	$\delta$	$A$	$T$	$\delta$	$A$	$T$	$\delta$	$A$
LLLLLL	2	4-pixel	1	0.5	0.2504	1.5	0.6	0.2227	1	0.5	0.2385
LLLLLL	2	8-pixel	1.5	0.4	0.2673	1.5	0.4	0.2442	1.5	0.4	0.2684
LLLLHL	2	8-pixel	3	0.5	0.2238	1.5	0.4	0.3560	1	0.3	0.3208
LLLLLH	2	8-pixel	2	0.4	0.2720	1.5	0.3	0.2834	1.5	0.3	0.2803
LLLLHH	2	8-pixel	3	0.5	0.2602	2.5	0.5	0.2732	2.5	0.5	0.3110
LLLLLL	3	8-pixel	1.5	0.2	0.2397	1.5	0.2	0.2217	1.5	0.2	0.2372
LLLLHL	3	8-pixel	1	0.1	0.2144	1	0.1	0.3395	1	0.1	0.3046
LLLLLH	3	8-pixel	1	0.1	0.2641	1	0.1	0.2766	1	0.1	0.2704
LLLLHH	3	8-pixel	1	0.1	0.2488	1	0.1	0.2613	1	0.1	0.3057

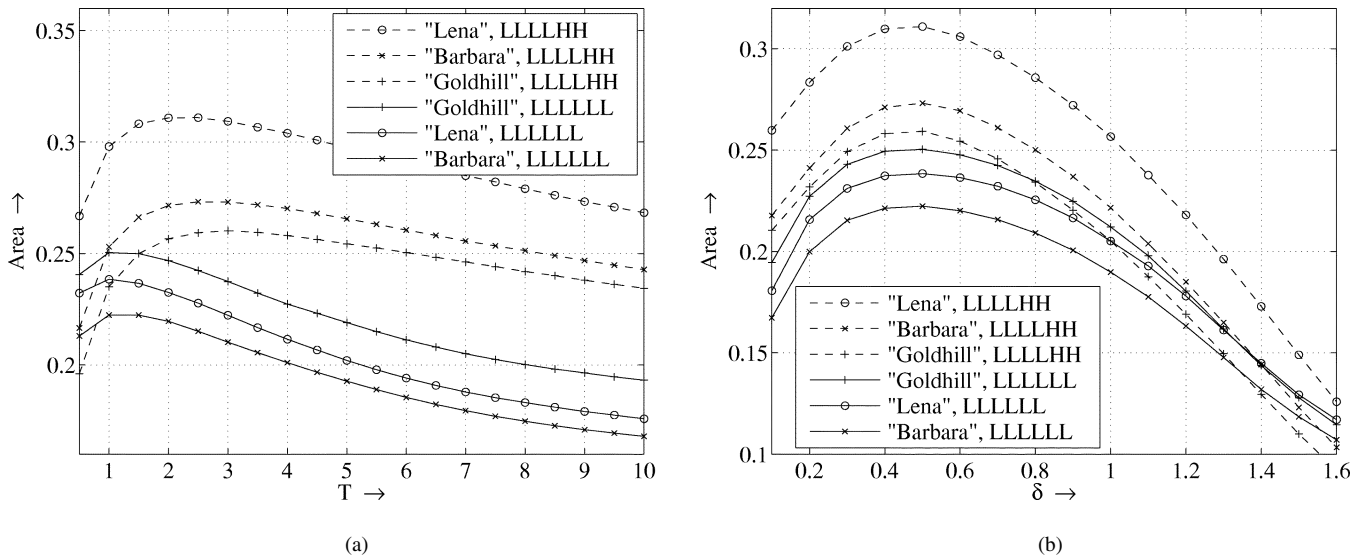


Fig. 6. Area under the EXIT function  $I_{E_o} = T_o(I_{A_o})$  for the MRF-based source decoder for the best cases in Table I ( $N_E = 2$ ,  $M = 6$  bits,  $N_{i,\text{MRF}} = 0$ , three-level wavelet filter bank, four-pixel neighborhood for the LLLLLL subband, eight-pixel neighborhood for the LLLLHH subband): (a) area versus temperature parameter  $T$  ( $\delta = 0.5$ ); (b) area versus parameter  $\delta$  ( $T = 1$  for the LLLLLL subband,  $T = 2.5$  for the LLLLHH subband).

different quantized subbands and test images the corresponding parameters  $T$  and  $\delta$  leading to the largest area  $A$ . We can observe that including three-element cliques gives inferior results in all cases such that we only consider two-element cliques for the simulations in Section V. Furthermore, for the LLLLLL subband and  $N_E = 2$  results are included in Table I for both four-pixel and eight-pixel neighborhoods, where the latter case gives a larger value of  $A$ . However, since according to Fig. 4 a four-pixel neighborhood leads to a larger average extrinsic information  $I_{E_o}$  for  $I_{A_o} = 1$  bit, it may be advantageous to only use horizontal and vertical cliques due to a potentially larger achievable extrinsic information in the convergence point. On the other hand, if  $C_B$  is present, then  $I_{E_o}(I_{A_o} = 1 \text{ bit}) = 1$  bit holds according to Theorem 1 below, such that it is rather preferable to obtain a larger  $A$  by means of an eight-pixel neighbor-

hood in order to possibly reduce the number of decoding iterations until convergence and to find a good matching inner code more easily.

Finally, for the LLLLLL band with  $N_E = 2$  and a four-pixel neighborhood and the LLLLHH band with  $N_E = 2$  and an eight-pixel neighborhood, respectively, Fig. 6(a) exemplarily shows the area  $A$  as a function of  $T$  for a fixed  $\delta = 0.5$ . We observe that especially in the highpass subband, the exploitable source redundancy is quite invariant to changes of  $T$ . Experiments have shown that this also holds for the LLLLHL and LLLLH subbands. Fig. 6(b) displays the area  $A$  versus  $\delta$  where according to Table I, a value of  $T = 1$  was chosen for the LLLLLL subband and of  $T = 2.5$  for the LLLLHH subband, respectively. Here, a mismatch of  $\delta$  by  $\pm 0.2$  only leads to a small decrease of the area  $A$  under the EXIT chart.

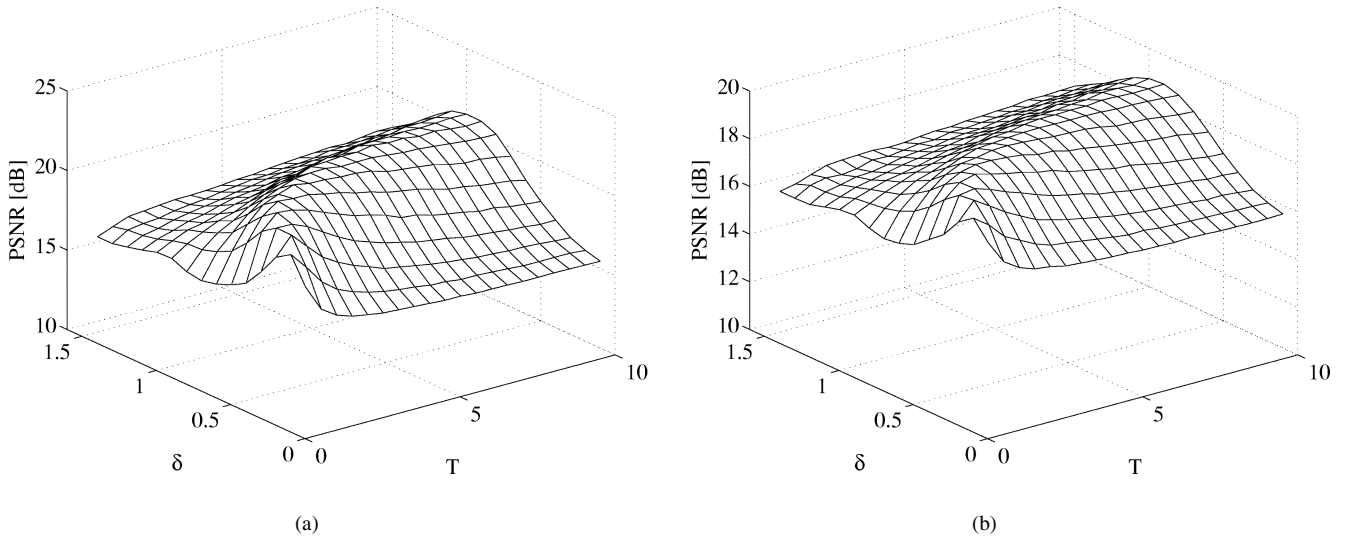


Fig. 7. PSNR versus MRF parameters  $T$  and  $\delta$  for  $E_b/N_0 = 1$  dB with  $E_b = E_s/(R_C R_B R_S)$  (LLLLLL subband quantized with  $M = 6$  bits,  $N_E = 2$ ,  $N_{i,\text{MRF}} = 0$ , three-level wavelet filter bank, four-pixel neighborhood, no outer block code, rate-2/3 RSC code as inner channel code): (a) “Goldhill” test image; (b) “Barbara” test image.

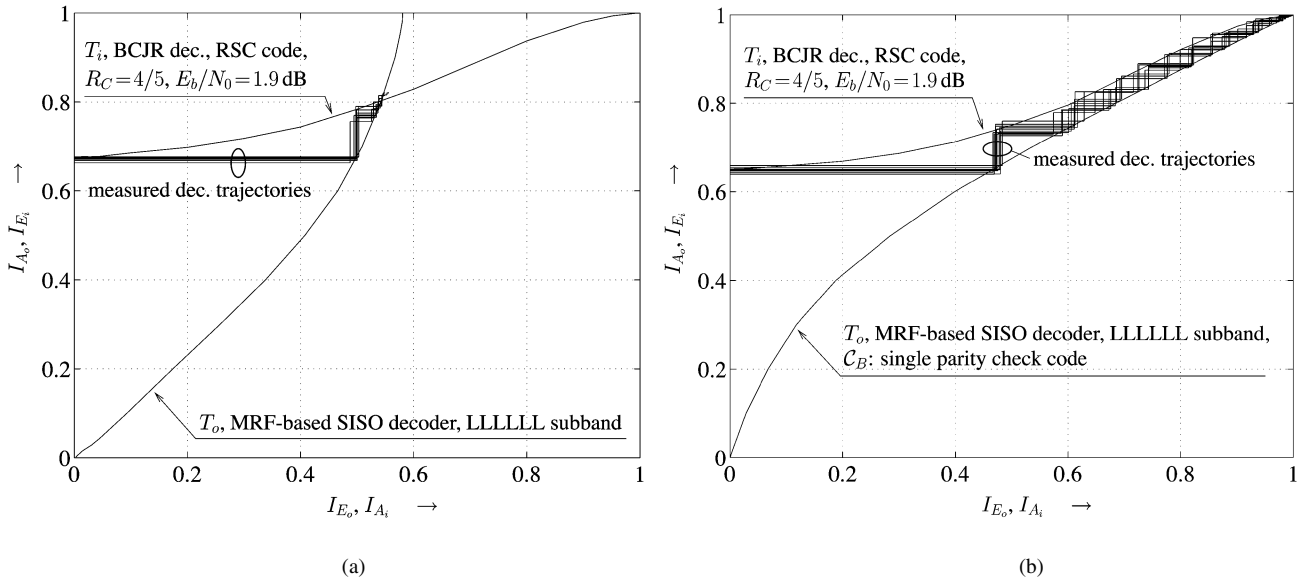


Fig. 8. EXIT chart for the outer MRF-based SISO source decoder (LLLLLL subband image, “Goldhill,”  $M = 6$  bit quantization) and the inner BCJR channel decoder (RSC code with  $R_C = 4/5$ , block length 24579 bits including termination bits for the RSC code): (a) no block code ( $\mathbf{G} = \mathbf{I}_M$ ),  $N_{i,\text{MRF}} = 3$ ; (b) with a single parity check ( $\mathbf{G} = [\mathbf{I}_M \mathbf{1}_M]$ ,  $R_B = 6/7$ ),  $N_{i,\text{MRF}} = 0$ .

We now verify that a large area  $A$  under the MRF-decoder’s EXIT characteristic is directly connected with a large peak-SNR (PSNR) after reconstruction. Fig. 7 shows the PSNR dependency on the MRF parameters  $T$  and  $\delta$  for the LLLLLL subband of “Lena” and “Barbara,” respectively, and the same MRF parameters as in Fig. 5. The simulations are carried out for  $E_b/N_0 = 1$  dB, where  $E_b = E_s/(R_C R_B R_S)$ ; the parameter  $E_b/N_0$  allows for a fair comparison of systems with different code rates. Additionally, no outer block code, but a rate-2/3 inner recursive systematic convolutional (RSC) code is employed, where six source-channel decoder iterations are performed. We can see that both the plots in Figs. 5 and 7 have similar shape with a “ridge” approximately for the same combinations of  $\delta$  and  $T$ , and thus, a large  $A$  also leads to a large PSNR. This also holds for different channel SNRs where

for larger  $E_b/N_0$  the “ridge” of the mesh plots in Fig. 7 is wider and narrower for smaller  $E_b/N_0$  on the channel, respectively.

We can now combine the EXIT function  $T_o$  for the MRF source decoder with the EXIT function  $T_i$  for the channel decoder. An example is depicted in Fig. 8(a) for  $E_b/N_0 = 1.9$  dB. As channel code, a memory-4 rate-1/4 RSC mother code taken from [32] with code polynomials  $(g_r, g_2, g_3, g_4) = (31, 27, 35, 33)_8$  is used, where  $g_r$  denotes the feedback polynomial and  $g_2, g_3, g_4$  the feedforward polynomials, respectively. By puncturing this mother code a whole RCPC code family with different rates can be constructed [32], which will be used for the image transmission example in Section V. In this example, this mother code is punctured to the rate  $R_C = 4/5$  by using the puncturing pattern  $[1, 1, 1, 1; 1, 0, 0, 0; 0, 0, 0, 0; 0, 0, 0, 0]$ . In order to illustrate the decoding process, Fig. 8 also

contains measured decoding trajectories. We can see that also for the MRF-based outer SISO decoder EXIT charts predict the convergence behavior quite accurately, where after three iterations convergence is already achieved. Besides, from the EXIT characteristics in Figs. 4 and (8a), it can be observed that for the MRF-based decoder the achieved average extrinsic information is always smaller than one, even when perfect *a priori* information (corresponding to  $I_{A_o} = 1$  bit) is available. The reason is given in the following theorem.

*Theorem 1:* Let  $I_{E_o,k} = (1/N) \sum_{\ell=1}^N I(B_{k,\ell}; L_{\text{extr}}^{(S)}(B_{k,\ell}))$  denote the average extrinsic information at the output of an (outer) SISO APP source decoder for some fixed  $k$ . Let furthermore  $H(B_{k,\ell}) = 1$  bit, and let  $d_{\min}$  denote the minimum Hamming distance between the  $2^M$  number of  $N$ -bit source codewords  $b_k \in \mathcal{B}$  of the code  $\mathcal{C}_B$ . Then,  $d_{\min} \geq 2$  is a necessary and sufficient condition for achieving  $I_{E_o,k}(I_{A_o,k} = 1 \text{ bit}) = 1$  bit.

The proof is given in the Appendix.

Since the source codewords  $i_k \in \mathcal{I}$ , in their binary representations, have a minimum mutual Hamming distance of  $d_{\min} = 1$ , we cannot reach  $I_{E_o}(I_{A_o} = 1 \text{ bit}) = 1$  bit due to Theorem 1. Furthermore, the overall average information available at the convergence point in Fig. 8(a) for the source decoder, which can be obtained by information combining of  $I_{A_o}$  and  $I_{E_o}$  [33], is also smaller than one. Ideally, we would like to reach the point  $(I_{E_o}, I_{A_o}) = (1 \text{ bit}, 1 \text{ bit})$  in the EXIT chart which leads to an overall average information of one bit at the constituent decoders and thus corresponds to an infinitesimally small bit error rate (BER). According to Theorem 1, we should increase  $d_{\min}$ , which can be achieved by appending the parity bits  $p_k$  of the code  $\mathcal{C}_B$  to the source index  $i_k$ . Especially, if just a single parity check is used with  $\mathbf{G} = [\mathbf{I}_M \ \mathbf{1}_M]$ , where  $\mathbf{1}_M$  denotes a column vector of  $M$  ones, the indexes  $i_k$  are just extended by one parity bit, which leads to a minimum Hamming distance  $d_{\min} = 2$  between the binary representation of the codeword indexes  $b_k$ . The result, which comes at the expense of a slightly higher overall rate, can be observed from the EXIT chart in Fig. 8(b). The EXIT function  $T_o$  for the MRF-based source decoder now exhibits the property  $T_o(1) = 1$ , and at the convergence point, an infinitesimally small BER for  $E_b/N_0 = 1.9$  dB can be obtained.

## V. SIMULATION RESULTS

In order to show the performance of the MRF-based source decoder for the reconstruction of channel-encoded images, the iterative source-channel decoder from Section IV will be applied to a simple image transmission system in the following. In this system the transmission model from Fig. 1 is used individually for every subband of a three-level wavelet filter bank. The allocation of the quantizer resolutions and the channel code rates is carried out by means of the rate allocation procedure proposed in [19]. This approach is based on the rate-distortion optimal bit allocation algorithm from [34], which is modified such that also the error correction capabilities of the channel codes and the additional channel noise are incorporated in the overall distortion measure. As convolutional codes  $\mathcal{C}_C$

terminated RSC codes derived from a memory-4 nonrecursive RCPC code family given in [32] are used, where the corresponding rate-1/4 mother code with code polynomials  $(g_r, g_2, g_3, g_4) = (31, 27, 35, 33)_8$  has already been utilized in the examples of Fig. 8. By applying different puncturing patterns, code rates of  $R_C \in \{8/9, 4/5, 2/3, 4/7, 1/2, 4/9, 4/10\}$  can be achieved. For those subbands where  $R_C = 1$  is assigned, a memory-3 rate-1/2 RSC mother code with generator polynomials  $(g_r, g_0)_8 = (15, 10)_8$  and the puncturing pattern  $[1, 0, 0; 0, 1, 1]$  is used, which has been found experimentally. We compare the following strategies to obtain the most important MRF parameters  $T$  and  $\delta$  at the source decoder.

- 1) The MRF parameters are derived from a training set of 20 natural images, where the test images “Goldhill” and “Lena” are not part of this set. The best parameters  $T$  and  $\delta$  maximizing the area  $A$  under the EXIT characteristic are determined for each subband image from the training set. The average  $T$  and  $\delta$  per subband are stored as universal parameters in the decoder.
- 2) The optimal parameters  $T$  and  $\delta$  are determined for each source image in the encoder and are transmitted as additional side information for each subband, which is allocated a nonzero amount of bits. Note that due to the large correlation between  $\delta$  and  $T$  (see Figs. 5 and 7), the amount of bits required for transmitting these parameters may be strongly reduced.

Furthermore, in the simulations we use an overall target bit rate of  $R_T = 0.37$  bits per pixel (bpp) including channel coding. It is assumed that besides the MRF parameters, the remaining side information, such as mean of the LLLLLL subband coefficients, and for each subband the quantizer scaling factors, the quantizer bit allocations, and the channel coding rates, are received without errors at the decoder. This may be carried out by protecting the side information by a low-rate (block) code. In this case, the additional overhead due to the transmission of side information amounts up to 0.5%–1% of the overall encoded data, where the larger figure corresponds to the case 2 from above. In the first setup, denoted with “MRF JSCD” in the following, a block code  $\mathcal{C}_B$  is not employed. We also consider the case where a single parity check with  $\mathbf{G} = [\mathbf{I}_M \ \mathbf{1}_M]$  is used after quantization, where this method will be referred to as “MRF JSCD SPC.” MRF parameters derived via a training set are indicated with the suffix “Tr.” (case 1), whereas transmitting them as side information is denoted with the suffix “best” (case 2).

The performance of the MRF approach is compared with the method from [15] (“2-D JSCD”) utilizing soft-input source decoding (SISD) [25], where a 2-D Markov model is used. The decoding is then carried out by a modified BCJR algorithm on the combined trellis for the Markov models. Average horizontal and vertical index transition probabilities are estimated from a large training set, stored in the decoder as *a priori* information, and used for every subband image pixel. In the “2-D JSCD” approach, the same rate allocation strategy, the same RCPC code family with the rate 1/4 mother code from above, and a similar iterative source-channel decoding setup are used. Furthermore, the same parameters as in the “MRF JSCD” case must be transmitted as side information except the MRF parameters  $T$  and  $\delta$ .

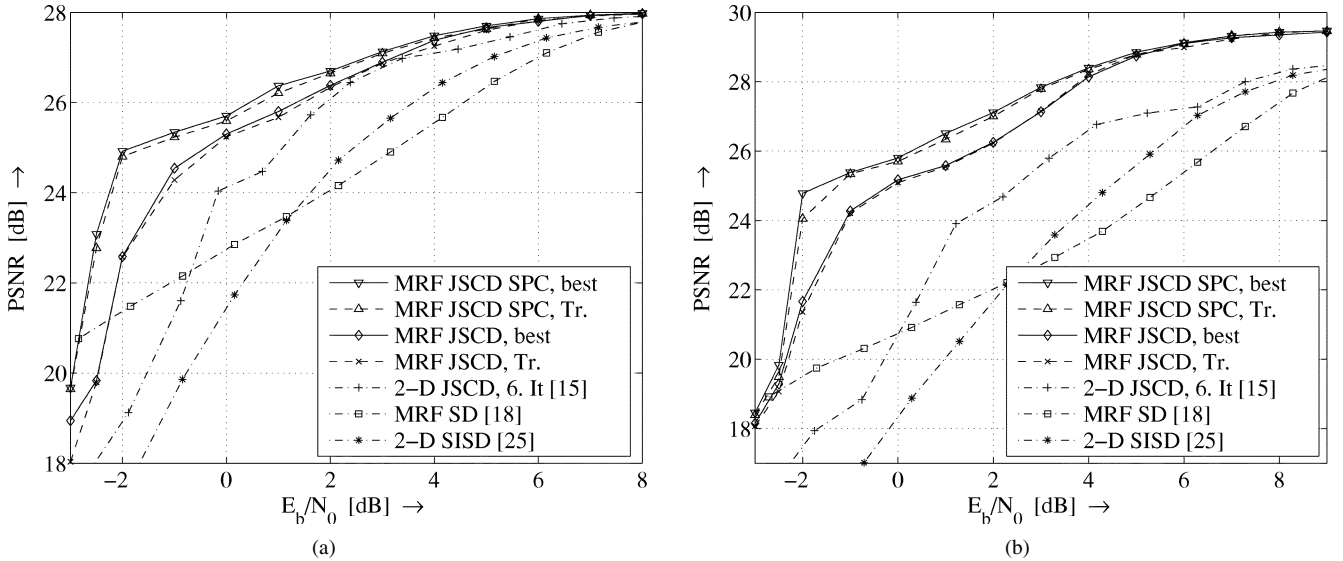


Fig. 9. PSNR versus  $E_b/N_0$  ( $R_T = 0.37$  bpp, three-level wavelet decomposition: (a) “Goldhill” image; (b) “Lena” image. A maximum of six source-channel decoder iterations was used for “MRF JSCD” and of 15 iterations for the “MRF JSCD SPC” approach, respectively.

Besides, both plain MRF-based source decoding (“MRF SD”) [18] and the “2-D SISD” approach [25] without additional protection by any channel code are also considered for comparison. For all approaches, an MS estimation of the subband image samples is employed.

Fig. 9(a) shows the simulation results<sup>5</sup> for the “Goldhill” image and the approaches described above. The PSNR values of the reconstructed images are averaged over 100 simulated transmissions for each  $E_b/N_0$  value, where  $E_b = E_s/R$  represents the transmit energy per information bit. The (overall) code rate  $R$  for the given system is obtained as

$$R = \frac{\sum_{\kappa=1}^K \eta_{\kappa}}{\sum_{\kappa=1}^K \frac{\eta_{\kappa}}{R_{C_{\kappa}} R_{B_{\kappa}} R_{S_{\kappa}}}} \quad \text{with} \quad R_{S_{\kappa}} = \frac{H(I_{\kappa,k} | I_{\kappa,k-1})}{M_{\kappa}}. \quad (19)$$

Herein,  $K$  denotes the overall number of subbands,  $\eta_{\kappa}$  the total number of data bits in the  $\kappa$ th subband after quantization, and  $R_{B_{\kappa}}$ ,  $R_{C_{\kappa}}$ , and  $R_{S_{\kappa}}$  the corresponding source and channel coding rates in the  $\kappa$ th subband. The source coding rate  $R_{S_{\kappa}}$  considers the implicit redundancy due to the residual index correlations in the  $\kappa$ th subband image, with  $I_{\kappa,k}$  describing an index of the serialized subband image data quantized with  $M_{\kappa}$  bits. As an example, for the “MRF JSCD” case with  $E_b/N_0 = 1$  dB,  $R_T \approx 0.37$  bit per pixel, and the  $512 \times 512$  “Goldhill” test image the rate allocation yields the following subband channel code rates and quantizer bit allocations: LLLLLL:  $R_{C_1} = 4/7$ ,  $M_1 = 6$ , LLLLHL:  $R_{C_2} = 1$ ,  $M_2 = 4$ , LLLLLH:  $R_{C_3} = 1$ ,  $M_3 = 5$ , LLLLHH:  $R_{C_4} = 1$ ,  $M_4 = 4$ ; the remaining subbands for  $\kappa = 5, \dots, 10$  are not transmitted. This leads to an overall code rate of  $R = 0.45$  for the whole image.

<sup>5</sup>The rate allocation algorithm being employed in these experiments only searches for operation points on the convex hull in the rate-distortion plane [19], [34]. Therefore, for some values of  $E_b/N_0$ , we obtain an overall bit rate being slightly smaller than the target rate  $R_T$ , and the curves for the JSCD techniques in Fig. 9 lack the smooth behavior of those for the pure MRF and 2-D SISD source decoding approaches.

For both the “MRF JSCD” and “MRF JSCD SPC” approaches  $N_{i,\text{MRF}} = 3$  MRF decoder iterations were used, which leads to comparable source decoder complexity. The maximum number of allowed source-channel decoder iterations was set to be six for “MRF JSCD” and 15 for “MRF JSCD SPC,” respectively, which is typically sufficient to achieve convergence for low channel SNR. However, for larger channel SNR, convergence is often achieved for a smaller number of iterations in both the MRF-based source decoder and the source-channel decoder.

We can observe from Fig. 9 for both the “Goldhill” [Fig. 9(a)] and “Lena” [Fig. 9(b)], test images using universal MRF parameters  $T$  and  $\delta$  derived from a training set in the decoder almost yields the same PSNR values as transmitting the best parameters separately for each image as side information. In Fig. 9(a), the “MRF JSCD SPC” techniques achieves a PSNR gain between 0.2 and 2 dB over the “MRF JSCD” approach for  $-2 \text{ dB} \leq E_b/N_0 \leq 0 \text{ dB}$ . Especially for low-channel SNR, the latter scheme also yields up to 1–2 dB larger PSNR compared with the “2-D JSCD” technique which, besides the larger memory demand, also exhibits a larger source decoding complexity of  $O(2^{2M})$  compared with  $O(2^M)$  for the MRF-based schemes as stated in Section III.

A possible reason for the improved performance could be that the proposed method employs a neighborhood which, except for the LLLLLL subband, completely surrounds the pixel under consideration. In contrast, the “2-D JSCD” technique considers a smaller neighborhood that only comprises the horizontally and vertically adjacent pixels in each subband image. The advantage of the MRF-based approaches may also be observed by comparing the “MRF SD” with the “2-D SISD” method, where for low-channel SNR, the MRF-based decoder outperforms the “2-D SISD” approach.

Compared with the plain source decoding approaches, we can see from the simulation results that in the best case we can gain up to 4 dB in PSNR for the *same* target rate  $R_T$  by adding explicit redundancy from channel codes in combina-



Fig. 10. Reconstructed “Goldhill” image example ( $R_T = 0.37$  bpp, three-level wavelet decomposition, “MRF JSCD SPC, best,”  $N_{i,\text{MRF}} = 1$ ): (a)  $E_b/N_0 = 1$  dB (overall code rate  $R = 0.45$ , equivalent to a codebit error rate of 14.4% on the channel), PSNR: 26.38 dB, six source-channel decoder iterations; (b)  $E_b/N_0 = -2$  dB (overall code rate  $R = 0.27$ , equivalent to a codebit error rate of 28% on the channel) PSNR: 25.29 dB, 15 source-channel decoder iterations.  $E_b$  contains the rate contribution from both the channel codes and the residual source redundancy.

tion with a joint rate allocation at the encoder and an iterative source-channel decoder. For the “Lena” test image in Fig. 9(b), similar observations can be made, where we can see that the largest gain of the “MRF JSCD SPC” approaches can again be obtained for strongly distorted channels. Examples of the good reconstruction quality for highly corrupted channels are given for the “Goldhill” image in Fig. 10.

## VI. CONCLUSION AND FINAL NOTES

We have derived a SISO source decoder that is able to exploit, e.g., the implicit 2-D residual source redundancy inherent in quantized subband images. The novelty is that the source signals are modeled using Markov random fields, and due to the Markov–Gibbs correspondence the computation of *a posteriori* probabilities serving as soft outputs can be made very resource- and complexity-efficient. In conjunction with channel coding, the proposed source decoder can be used as an outer constituent decoder in an iterative decoding scheme. However, in this plain form, such a scheme suffers from the fact that the source decoder is not able to deliver the maximum possible extrinsic information at its output even when perfect *a priori* information is applied. As a remedy, we suggest to apply a high-rate block code to the quantized source indexes and jointly decode the MRF and the block code in the source decoder. With this method, a minimum distance larger than one between the source codewords is achieved, and it is shown that this leads to an increased performance of the iterative decoder. As an example, we have applied the proposed source-channel decoding technique to robust image transmission over very noisy AWGN channels, where PSNR values of over 25 dB can still be obtained for a channel SNR of  $-2$  dB in  $E_b/N_0$ .

Finally, we note that the presented MRF-based source decoder may also be used for exploiting the 2-D spatial redundancy when additional variable-length source encoding is present. This setup then represents a triple serial concatenation of implicit 2-D source redundancy (and possibly the high-rate block code  $\mathcal{C}_B$ ), the variable-length code (VLC) source encoder, and the channel encoder  $\mathcal{C}_C$ . A suitable decoder may then, on the one hand, carry out index-based iterations between the MRF-based source decoder and an index-based VLC SISO source decoder (see, e.g., [35]), and on the other hand, iterate between SISO channel and VLC source decoder. Furthermore, the proposed MRF source decoding approach can not only be applied to 2-D (subband) images; it may also be used to exploit 2-D parameter correlations, e.g., from source codec parameters which exploit both interframe and intraframe redundancy.

## APPENDIX PROOF OF THEOREM 1

The average extrinsic information  $I_E := I_{E_o,k}$  at the output of the (outer) source decoder can be expressed as

$$I_E = \frac{1}{N} \sum_{\ell=1}^N I(X_\ell; E_\ell) = \frac{1}{N} \sum_{\ell=1}^N H(X_\ell) - H(X_\ell|E_\ell) \quad (20)$$

with the abbreviations  $E_\ell := L_{\text{extr}}^{(S)}(B_{k,\ell})$  and  $X_\ell := B_{k,\ell}$ . Furthermore, for the sake of clarity, we will omit the time index  $k$  in what follows.

In [28], it is shown that, when an outer SISO decoder emitting true APPs is used in a serially concatenated scheme, the mutual

information  $I(X_\ell; E_\ell)$  can also be written with the assumption  $H(X_\ell) = 1$  bit as

$$I(X_\ell; E_\ell) = I(X_\ell; \hat{\mathbf{W}}_{[\ell]}) = 1 - H(X_\ell | \hat{\mathbf{W}}_{[\ell]}) \quad (21)$$

where  $\hat{\mathbf{W}}_{[\ell]} = [\hat{W}_1, \dots, \hat{W}_{\ell-1}, \hat{W}_{\ell+1}, \dots, \hat{W}_N]$  describes the received soft-bit sequence at the output of the *a priori* AWGN channel<sup>6</sup> with noise variance  $\sigma_A^2$  and capacity  $I_A(\sigma_A)$ . The L-values at the *a priori* channel output can be identified as  $L_a^{(S)}(b_k, \ell)$  in Fig. 3. In the sequel the subscript “[ $\ell$ ]” will indicate that the  $\ell$ th bit is excluded from a sequence or from all elements in a set.

The conditional entropy  $H(X_\ell | \hat{\mathbf{W}}_{[\ell]})$  in (21) may now be further expanded as

$$H(X_\ell | \hat{\mathbf{W}}_{[\ell]}) = - \int_{-\infty}^{\infty} \sum_{x=0}^1 \sum_{\forall b \in \mathcal{B}: b_\ell = x} [p(\hat{\mathbf{w}}_{[\ell]} | b) P(b)] \times \log_2 \left( \frac{1}{p(\hat{\mathbf{w}}_{[\ell]})} \sum_{\forall b \in \mathcal{B}: b_\ell = x} p(\hat{\mathbf{w}}_{[\ell]} | b) P(b) \right) d\hat{\mathbf{w}}_{[\ell]} \quad (22)$$

with

$$p(\hat{\mathbf{w}}_{[\ell]}) = \sum_{\forall b' \in \mathcal{B}: b'_\ell = 0} p(\hat{\mathbf{w}}_{[\ell]} | b') P(b') + \sum_{\forall b' \in \mathcal{B}: b'_\ell = 1} p(\hat{\mathbf{w}}_{[\ell]} | b') P(b'). \quad (23)$$

With  $\tilde{\sigma}_A^2 = 4/\sigma_A^2$ , the following properties for  $I_A$  can be stated [22]:  $\lim_{\tilde{\sigma}_A \rightarrow 0} I_A(\tilde{\sigma}_A) = 0$  bit,  $\lim_{\tilde{\sigma}_A \rightarrow \infty} I_A(\tilde{\sigma}_A) = 1$  bit. The latter case for  $\tilde{\sigma}_A \rightarrow \infty$  yields

$$p(\hat{\mathbf{w}}_{[\ell]} | b) \Big|_{\tilde{\sigma}_A \rightarrow \infty} = \prod_{\forall \xi \in \{1, 2, \dots, N\} \setminus \ell} \delta_0(\hat{w}_\xi - (1 - 2b_\xi)) \quad (24)$$

where  $\delta_0(\cdot)$  denotes the Dirac impulse. With  $\nu_\lambda \in \{0, 1\}$  for  $\lambda \in \{1, 2, \dots, N\}$ , we now define the sequences  $\boldsymbol{\nu}_{[\ell]} = [\nu_1, \dots, \nu_{\ell-1}, \nu_{\ell+1}, \dots, \nu_N]$  and  $\boldsymbol{\nu}_{\ell \rightarrow x} = [\nu_1, \dots, \nu_{\ell-1}, x, \nu_{\ell+1}, \dots, \nu_N]$ . Inserting (24) in (22) with (23) yields

$$H(X_\ell | \hat{\mathbf{W}}_{[\ell]}) \Big|_{\tilde{\sigma}_A \rightarrow \infty} = - \sum_{\forall \boldsymbol{\nu}_{[\ell]} \in \mathcal{B}_{[\ell]}} \sum_{x=0}^1 P(b = \boldsymbol{\nu}_{\ell \rightarrow x}) \cdot \log_2 \left( \underbrace{\frac{P(b = \boldsymbol{\nu}_{\ell \rightarrow x})}{P(b = \boldsymbol{\nu}_{\ell \rightarrow 0}) + P(b = \boldsymbol{\nu}_{\ell \rightarrow 1})}}_{=: A_\ell} \right). \quad (25)$$

<sup>6</sup>For the modeling of the *a priori* information, please see [21], [22], and [28].

*Necessary Condition:* In order to achieve  $I_E = 1$  bit for  $\tilde{\sigma}_A \rightarrow \infty$ , it follows from (20) and (21) that  $H(X_\ell | \hat{\mathbf{W}}_{[\ell]}) \Big|_{\tilde{\sigma}_A \rightarrow \infty} \stackrel{!}{=} 0$  bit for all  $\ell = 1, 2, \dots, N$ . When we assume that  $P(b) \neq 0$  for all  $b \in \mathcal{B}$ , this can only be achieved by  $A_\ell = 0$  in (25). This is satisfied if the index  $b = \boldsymbol{\nu}_{\ell \rightarrow (1-x)}$ , where the bit  $x \in \{0, 1\}$  is replaced by the bit  $1 - x$ , does not correspond to a codeword. Since  $\mathcal{C}_B$  is a linear code, we only need to consider the all-zero codeword  $b = \boldsymbol{\nu}_{\ell \rightarrow 0}^{(0)} = [0, \dots, 0]$ . In order to achieve  $A_\ell = 0$ , we demand  $\boldsymbol{\nu}_{\ell \rightarrow 1}^{(0)} \notin \mathcal{B}$  to hold for the index  $b = \boldsymbol{\nu}_{\ell \rightarrow 1}^{(0)}$  with Hamming weight  $w(\boldsymbol{\nu}_{\ell \rightarrow 1}^{(0)}) = 1$  for all  $\ell \in \{1, 2, \dots, N\}$ . However, this necessarily leads to  $d_{\min} \geq 2$  for the code  $\mathcal{C}_B$ .

*Sufficient Condition:* If  $d_{\min} \geq 2$  is given, we have  $A_\ell = 0$  in (25), which results in  $H(X_\ell | \hat{\mathbf{W}}_{[\ell]}) \Big|_{\tilde{\sigma}_A \rightarrow \infty} = 0$  bit for all  $\ell \in \{1, 2, \dots, N\}$ . With (20) and (21), this leads to  $I_E = 1$  bit.  $\square$

#### ACKNOWLEDGMENT

The authors would like to thank the anonymous reviewers for several valuable suggestions, which helped to improve the paper.

#### REFERENCES

- [1] K. Sayood and J. C. Borkenhagen, "Use of residual redundancy in the design of joint source/channel coders," *IEEE Trans. Commun.*, vol. 39, no. 6, pp. 838–846, Jun. 1991.
- [2] J. Hagenauer, "Source-controlled channel decoding," *IEEE Trans. Commun.*, vol. 43, no. 9, pp. 2449–2457, Sep. 1995.
- [3] H. H. Otu and K. Sayood, "A joint source/channel coder with block constraints," *IEEE Trans. Commun.*, vol. 47, no. 22, pp. 1615–1618, Nov. 1999.
- [4] M. Park and D. J. Miller, "Improved image decoding over noisy channels using minimum mean-squared estimation and a Markov mesh," *IEEE Trans. Image Process.*, vol. 8, no. 6, pp. 863–867, Jun. 1999.
- [5] T. Fingscheidt and P. Vary, "Softbit speech decoding: a new approach to error concealment," *IEEE Trans. Speech Audio Process.*, vol. 9, no. 3, pp. 240–251, Mar. 2001.
- [6] P. G. Sherwood and K. Zeger, "Error protection for progressive image transmission over memoryless and fading channels," *IEEE Trans. Commun.*, vol. 46, no. 12, pp. 1555–1559, Dec. 1998.
- [7] V. Chande and N. Farvardin, "Joint source-channel coding for progressive transmission of embedded source coders," in *Proc. IEEE Data Compression Conf.*, Snowbird, UT, Mar. 1999, pp. 52–61.
- [8] C. Lan, T. Chu, K. R. Narayanan, and Z. Xiong, "Scalable image and video transmission using irregular repeat-accumulate codes with fast algorithm for optimal unequal error protection," *IEEE Trans. Commun.*, vol. 52, no. 7, pp. 1092–1101, Jul. 2004.
- [9] Y. Wang and Q.-F. Zhu, "Error control and concealment for video communications: A review," *Proc. IEEE*, vol. 86, no. 5, pp. 974–997, May 1998.
- [10] S. Shirani, F. Kossentini, and R. Ward, "An error concealment method for video communications in an error-prone environment," *IEEE J. Sel. Areas Commun.*, vol. 18, no. 6, pp. 1122–1128, Jun. 2000.
- [11] S. S. Hemami and T. H.-Y. Meng, "Transform coded image reconstruction exploiting interblock correlation," *IEEE Trans. Image Process.*, vol. 4, no. 7, pp. 1023–1027, Jul. 1995.
- [12] P. Salama, N. B. Shroff, and E. J. Delp, "Error concealment in MPEG video streams over ATM networks," *IEEE J. Sel. Areas Commun.*, vol. 18, no. 6, pp. 1129–1144, Jun. 2000.
- [13] S. Geman and D. Geman, "Stochastic relaxation, Gibbs distribution, and the Bayesian restoration of images," *IEEE Trans. Pattern Anal. Machine Intell.*, vol. PAMI-6, no. 6, pp. 721–741, Nov. 1984.
- [14] L. R. Bahl, J. Cocke, F. Jelinek, and J. Raviv, "Optimal decoding of linear codes for minimizing symbol error rate," *IEEE Trans. Inf. Theory*, pp. 294–287, Mar. 1974.
- [15] J. Kliewer and N. Goertz, "Iterative source-channel decoding for robust image transmission," in *Proc. IEEE Int. Conf. Acoust., Speech, Signal Processing*, Orlando, FL, May 2002, pp. 2173–2176.

- [16] T. Fingscheidt, T. Hindelang, R. V. Cox, and N. Seshadri, "Joint source-channel (de-)coding for mobile communications," *IEEE Trans. Commun.*, vol. 50, no. 2, pp. 200–212, Feb. 2002.
- [17] N. Goertz, "On the iterative approximation of optimal joint source-channel decoding," *IEEE J. Sel. Areas Commun.*, vol. 14, no. 9, pp. 1662–1670, Sep. 2001.
- [18] A. Mertins, "Image recovery from noisy transmission using soft bits and Markov random field models," *Opt. Eng.*, vol. 42, no. 10, pp. 2893–2899, Oct. 2003.
- [19] J. Kliewer, N. Goertz, and A. Mertins, "Iterative source-channel decoding for error-resilient image transmission using a Markov random field source model," in *Proc. Int. ITG Conf. Source Channel Coding (SCC)*, Erlangen, Germany, Jan. 2004, pp. 305–310.
- [20] —, "On iterative source-channel image decoding with Markov random field source models," in *Proc. IEEE Int. Conf. Acoust., Speech, Signal Processing*, Montreal, QC, Canada, May 2004, pp. 661–664.
- [21] S. ten Brink, "Code characteristic matching for iterative decoding of serially concatenated codes," *Ann. Telecommun.*, vol. 56, no. 7–8, pp. 394–408, Jul.–Aug. 2001.
- [22] —, "Convergence behavior of iteratively decoded parallel concatenated codes," *IEEE Trans. Commun.*, vol. 49, no. 10, pp. 1727–1737, Oct. 2001.
- [23] C. A. Bouman and K. Sauer, "A generalized Gaussian image model for edge-preserving MAP estimation," *IEEE Trans. Inf. Theory*, vol. 2, no. 3, pp. 296–310, Jul. 1993.
- [24] P. H. Westerink, J. Biemond, and D. E. Boeke, "Subband coding of color images," in *Subband Image Coding*, J. W. Woods, Ed. Boston, MA: Kluwer, 1991, pp. 193–227.
- [25] J. Kliewer and N. Goertz, "Soft-input source decoding for robust transmission of compressed images using two-dimensional optimal estimation," in *Proc. IEEE Int. Conf. Acoust., Speech, Signal Processing*, Salt Lake City, UT, May 2001, pp. 2565–2568.
- [26] S. Benedetto, D. Divsalar, G. Montorsi, and F. Pollara, "Serial concatenation of interleaved codes: performance analysis, design, and iterative decoding," *IEEE Trans. Inf. Theory*, vol. 44, no. 3, pp. 909–926, May 1998.
- [27] J. Hagenauer, E. Offer, and L. Papke, "Iterative decoding of binary block and convolutional codes," *IEEE Trans. Inf. Theory*, vol. 42, no. 2, pp. 429–445, Mar. 1996.
- [28] A. Ashikhmin, G. Kramer, and S. ten Brink, "Extrinsic information transfer functions: Model and erasure channel properties," *IEEE Trans. Inf. Theory*, vol. 50, no. 11, pp. 2657–2673, Nov. 2004.
- [29] M. Tüchler and J. Hagenauer, "Exit charts of irregular codes," in *Proc. Conf. Information Sciences Systems (CISS)*, Princeton, NJ, Mar. 2002.
- [30] R. Thobaben and J. Kliewer, "Low-complexity iterative joint source channel decoding for variable-length encoded Markov sources," *IEEE Trans. Commun.*, vol. 53, no. 12, pp. 2054–2064, Dec. 2005.
- [31] R. G. Gallager, *Information Theory and Reliable Communication*. New York: Wiley, 1968.
- [32] J. Hagenauer, "Rate-compatible punctured convolutional codes (RCPC codes) and their applications," *IEEE Trans. Commun.*, vol. 36, no. 4, pp. 389–400, Apr. 1988.
- [33] I. Land, S. Huettinger, P. A. Hoehner, and J. Huber, "Bounds on information combining," *IEEE Trans. Inf. Theory*, vol. 51, no. 2, pp. 612–619, Feb. 2005.
- [34] Y. Shoham and A. Gersho, "Efficient bit allocation for an arbitrary set of quantizers," *IEEE Trans. Acoust., Speech, Signal Processing*, vol. 36, no. 9, pp. 1445–1453, Sep. 1988.
- [35] J. Kliewer and R. Thobaben, "Iterative joint source-channel decoding of variable-length codes using residual source redundancy," *IEEE Trans. Wireless Commun.*, vol. 4, no. 3, pp. 919–929, May 2005.



**Jörg Kliewer** (S'97–M'99–SM'04) received the Dipl.-Ing. degree in electrical engineering from the Hamburg University of Technology, Hamburg, Germany, in 1993 and the Dr.-Ing. degree (Ph.D.) in electrical engineering from the University of Kiel, Kiel, Germany, in 1999, respectively.

From 1993 to 1998, he was a Research Assistant at the Institute for Circuits and Systems Theory at the University of Kiel. In 1996, he spent five months at the Image Processing Laboratory, University of California, Santa Barbara, as a visiting Researcher. Since 1999, he has been a Senior Researcher and Lecturer with the Faculty of Engineering, University of Kiel. On leave from the University of Kiel, he was visiting the University of Southampton, U.K., for one year in 2004 and has been a Visiting Assistant Professor with the University of Notre Dame, IN, since 2005. His current research interests include joint source and channel coding, error correcting codes, and network coding.



**Norbert Goertz** (S'97–M'99–SM'03) received the Dipl.-Ing. degree in electrical engineering from the Ruhr-University Bochum, Germany, in 1993, the Dr.-Ing. (Ph.D.) degree from the University of Kiel, Kiel, Germany, in 1999, and the postdoctoral "Habilitation" degree from the Munich University of Technology, Munich, Germany, in June 2004.

In 1993, he joined the Department of Engineering of the University of Kiel as a Research Assistant, where he served as a Member of the Research Staff until October 2000. In November 2000, he joined the Munich University of Technology, Germany, as a Senior Researcher and Lecturer. From December 2003 until February 2003, he was a Visiting Researcher and Guest Lecturer at the Department of Information Technology, Lund University, Sweden. From April 2004 until September 2004, he was a temporary Professor for Communications and Radio Frequency Engineering at the University of Kassel, Germany. Since October 2004, he has been a Lecturer at the Institute for Digital Communications, Joint Research Institute for Signal & Image Processing, University of Edinburgh, Scotland, U.K. His research interests include source and channel coding, the application of the turbo principle in communications, and cross-layer system design for wireless networks.



**Alfred Mertins** (M'96–SM'03) received the Dipl.-Ing. degree from the University of Paderborn, Germany, in 1984 and the Dr.-Ing. degree in electrical engineering and the Dr.-Ing. Habil. degree in telecommunications from the Hamburg University of Technology, Hamburg, Germany, in 1991 and 1994, respectively.

From 1986 to 1991, he was with the Hamburg University of Technology; from 1991 to 1995 with the Microelectronics Applications Center Hamburg, Germany; from 1996 to 1997 with the University of Kiel, Germany; from 1997 to 1998 with the University of Western Australia; and from 1998 to 2003 with the University of Wollongong, Australia. In April 2003, he joined the University of Oldenburg, Oldenburg, Germany, where he is currently a Professor in the Faculty of Mathematics and Science. His research interests include speech, audio, image and video processing, wavelets and filter banks, and digital communications.